AIP | Review of Scientific Instruments

A multi-detector, digitizer based neutron depth profiling device for characterizing thin film materials

P. L. Mulligan, L. R. Cao, and D. Turkoglu

Citation: Rev. Sci. Instrum. **83**, 073303 (2012); doi: 10.1063/1.4732168
View online: http://dx.doi.org/10.1063/1.4732168
View Table of Contents: http://rsi.aip.org/resource/1/RSINAK/v83/i7
Published by the American Institute of Physics.

A multi-detector, digitizer based neutron depth profiling device for characterizing thin film materials

P. L. Mulligan, L. R. Cao,[a] and D. Turkoglu
Nuclear Engineering Program, Department of Mechanical and Aerospace Engineering, The Ohio State University, Columbus, Ohio 43210, USA

(Received 30 April 2012; accepted 14 June 2012; published online 6 July 2012)

Neutron depth profiling (NDP) is a mature, nondestructive technique used to characterize the concentration of certain light isotopes in a material as a function of depth by measuring the residual energy of charged particles in neutron induced reactions. Historically, NDP has been performed using a single detector, resulting in low intrinsic detection efficiency, and limiting the technique largely to high flux research reactors. In this work, we describe a new NDP instrument design with higher detection efficiency by way of spectrum summing across multiple detectors. Such a design is capable of acquiring a statistically significant charged particle spectrum at facilities limited in neutron flux and operation time. © *2012 American Institute of Physics*. [http://dx.doi.org/10.1063/1.4732168]

I. INTRODUCTION

Neutron depth profiling (NDP) is a nondestructive analytical technique used to determine the concentration of certain light isotopes in nearly any host material. The technique was first pioneered by Ziegler *et al.*[1] in 1972 to study boron implantations in silicon wafers, and later refined by Biersack *et al.*[2] to investigate other light elements with large neutron cross sections (e.g., ^{3}He, ^{6}Li, and ^{7}Be). Variations in instrumentation setups have been used to increase the resolution and sensitivity of NDP. Cold neutrons[3] and capillary optics[4] have been used to increase a reactive species cross section and neutron flux, respectively, for greater count rates. Additional techniques including large angle coincidence spectrometry[5] to increase NDP counting rates for low flux reactors, pulse-shape discrimination[6] for background reduction, and time-of-flight[7] measurements for greater energy resolution have also been implemented in other NDP instruments.

Historically, NDP has been accomplished using a charged particle spectrum obtained from a single detector and analog data acquisition systems. While multiple detectors have been used in NDP instruments, these setups were limited to only a few detectors, and the spectrum obtained in each channel was analyzed independently from one another. Performing NDP with a single detector is not problematic when high neutron flux and long acquisition periods are readily available. However, achieving reasonable counting statistics with single detector NDP instruments at low flux reactors with limited run times can be challenging. More precise counting statistics can be achieved by adding more detectors to the device, but the required shaping amplifier and multichannel analyzer (MCA) for each detector can be cost prohibitive. The advent of entirely digital data acquisition systems has made the implementation multi-detector systems cost effective, with energy resolution comparable to analog systems.[8] We propose a new instrumentation design utilizing a multi-detector, digital data acquisition system, to increase detection efficiency by summing spectra across multiple detector channels. Low power facilities may find utility in this design when a high count rate is a priority, while high power facilities might enjoy a more precise analysis by implementing this design with a grazing exit geometry.

II. PRINCIPLE OF NDP

NDP is based on the principle of detecting the residual energy of neutron induced charged particle reactions. When a sample is irradiated with a well collimated beam of thermal or cold neutrons, certain isotopes distributed throughout the material undergo exothermic reactions upon neutron absorption. Since neutron attenuation in the sample is negligible, the sample is uniformly exposed to neutrons at all depths. These reactions produce a charged particle and recoil nucleus of known kinetic energy, determined by the Q-value of the reaction. The isotropically emitted charged particle and recoil nucleus lose energy via electronic and nuclear interactions while travelling through the sample material. By measuring the residual energy of charged particles which escape the sample, the path length of the charged particles can be determined from the material's stopping power and

$$p = \int_{E(p)}^{E_0} \frac{1}{S(E)} dE, \tag{1}$$

where p is the path length, E_0 is the particle's initial energy, $E(p)$ is the residual energy after leaving the sample, and $S(E)$ is the stopping power of the sample material.[1] To prevent energy loss after particles have left the sample surface, NDP is performed in a vacuum environment. The stopping power of the sample material can be determined using the stopping and range of ions in matter (SRIM) code of Ziegler *et al.*[9] The average depth of the reaction is calculated from the path length of the charged particles using

$$x = \cos(\theta_p) p, \tag{2}$$

where x is the depth of the reaction, θ_p is the angle between the sample normal and detector (Fig. 1), and p is the path

[a]Author to whom correspondence should be addressed. Electronic mail: cao.152@osu.edu.

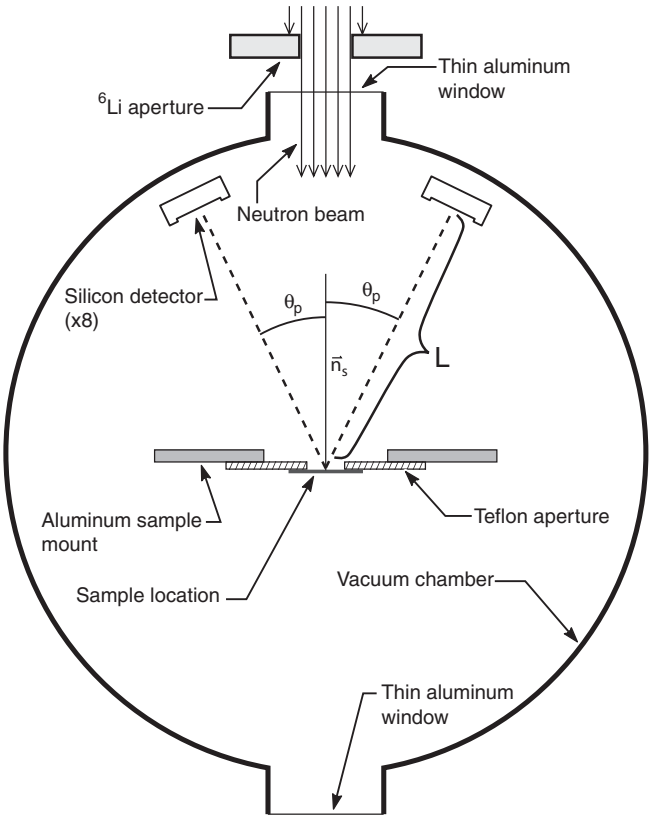

FIG. 1. Schematic view inside vacuum system of the NDP instrument. The adjustable arms holding each detector allow for a range of angles between detector and surface norms. θ_p for the experiments described in this paper was ≈26°, with L ≈12.2 cm.

length of the particle. By measuring the number of particles traversing a given path length, the concentration of that parent isotope can be determined for known neutron flux and detector efficiency or by way of comparison to a certified standard material. The production rate of ions from a depth x in the sample, for neutrons within energy dE about E is given by

$$F(x, E) = C(x) f_{ion} \sigma_{ion}(E) A_s \phi(E) dE, \quad (3)$$

where $C(x)$ is the areal density of the isotope of interest, A_s is the area of the sample illuminated by the neutron beam, $\phi(E)$ is the differential neutron flux, and f_{ion} and $\sigma_{ion}(E)$ are the fractional yield and reaction cross section of the ion of interest, respectively.[10]

The detection or count rate of ions from a depth x, induced by neutrons of energy E is related to the production rate through

$$N(x, E) = \frac{\Omega_d}{4\pi} \epsilon F(x, E), \quad (4)$$

where Ω_d is the solid angle subtended by a detector, and ε is the detector efficiency for an incident ion, typically equal to 1 for solid-state detectors. As the total neutron flux and energy distribution are typically fixed for a reactor, and consequently the reactive species cross section, the count rate for an NDP instrument can only be increased by augmenting A_s or Ω_d. Our design seeks to increase Ω_d by using a total of 8 detectors, summing the spectrum obtained from each independent detector channel.

While the uncertainty of an NDP analysis relies heavily on the experimental setup, of an equal importance is the method of spectrum deconvolution. Ziegler *et al.*[1] first used fast Fourier transforms to generate a response function for the detector, then integrated the stopping power of the substrate from the charged particle's initial energy to the final residual energy. The stopping power was calculated using a least-squares fit of data available at the time. Maki *et al.*[11] described two iterative methods for spectrum deconvolution, as they apply to NDP: chi-square minimization and Van Cittert. Chi-square minimization was found to successfully deconvolute NDP spectra, regardless of counting statistics, but requires an *a priori* knowledge of the depth profile. Van Cittert iterative deconvolution was also successful, but only for slowly varying distributions and required good counting statistics.

Coakley[12] adopted the iterative expectation maximization algorithm from emission tomography, and applied it to a simulated NDP spectrum with some success. A cross-validation procedure was added to the algorithm to prevent the creation of artifacts in the deconvoluted spectra, and was able to reconstruct the depth profile without prior knowledge. Several other methods for spectrum deconvolution have also been suggested, including the Simplex method[13] which includes a form of Tikhonov regularization utilizing a user generated regularization parameter. While the previous methods are limited to analyzing flat sample surfaces, work on deconvoluting ion spectra from curved surfaces has been done.[10]

III. SETUP

A. Beam facility

The Ohio State University research reactor (OSURR) provides the neutron source necessary for NDP. The OSURR (Fig. 2) is a 500 kW thermal, light water, open pool-type, research reactor with two radial beam ports. A collimator[14] composed of borated aluminum and lead disks for reduction in beam diameter, single-crystal sapphire for fast neutron filtering, and polycrystalline bismuth for gamma filtering is positioned in one of the two beam ports at the facility. The beam is turned on and off using a beam shutter made of a borated aluminum disk, borated polyethylene, and lead shielding. The beam line facility is enclosed by concrete bricks and the beam is terminated using a ^{6}Li epoxy disk at the end of a borated polyethylene and lead tunnel. Just before entering the vacuum chamber, the collimated beam is reduced in diameter using a SiO_2-LiO_2-CeO_2 glass aperture, containing 20.5% Li by mass, enriched in ^{6}Li to 95%. Interchangeable apertures of 10 mm and 30 mm are used for this final beam reduction, giving the beam a relatively flat neutron energy distribution at the sample position. Neutron activation analysis of a gold foil at the end of the beam collimator determined the neutron thermal equivalent flux to be $(1.27 \pm 0.03) \times 10^7$ n/cm^2 s, with a cadmium ratio of 266 ± 13.

B. NDP instrument

An integral component of the NDP instrument is the 61 cm × 61 cm right circular cylinder, stainless steel

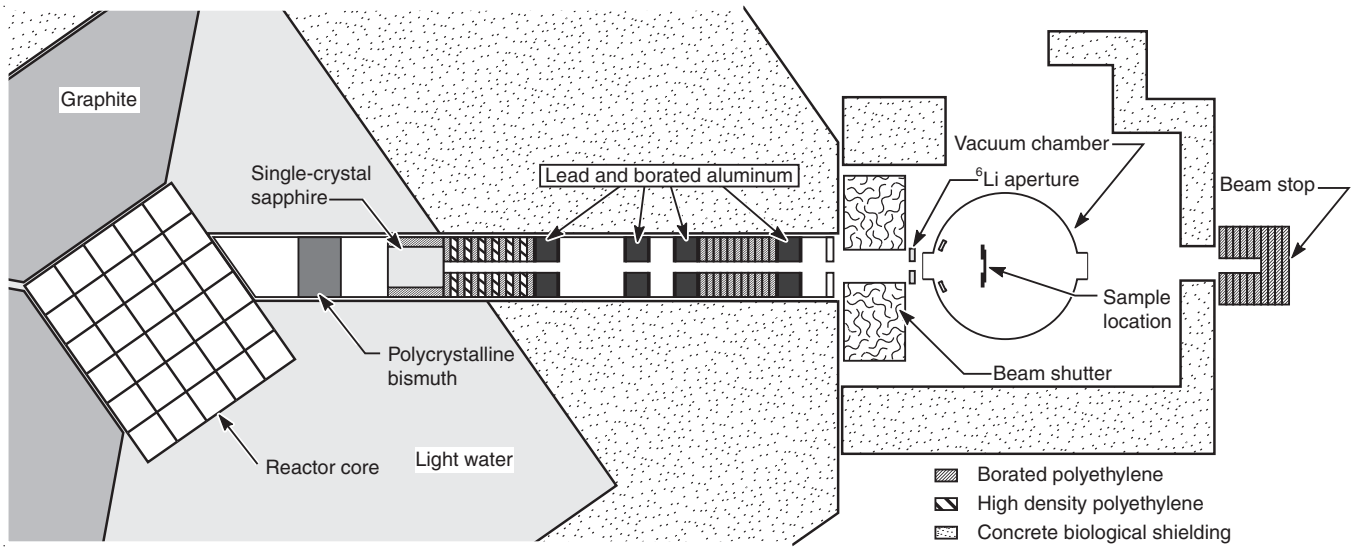

FIG. 2. Schematic of OSU research reactor, neutron beam collimator, and NDP instrument. The sample location is approximately 3.2 m from the edge of the reactor core. Figure not to scale.

304 vacuum chamber (Fig. 3). A 10^{-6} Torr pressure is maintained during profiling experiments with a turbomolecular pump and cold cathode vacuum gauge. To minimize beam scatter and attenuation through the chamber, a pair of 80 μm thin aluminum windows serves as the entrance and exit ports. Inside of the chamber lies an array of 8 silicon charged particle detectors, arranged annularly around the front entrance window. The detectors are placed on individually adjustable detector mounts (Fig. 4), located at the end of 8 adjustable arms. The adjustable arms permit a range of angles between sample surface and detector, ranging from approximately 20° to 90° (Fig. 1). Samples are placed on an aluminum disk centered in the neutron beam. Each detector is adjusted to face the sample location with approximately the same solid angle. Ortec ULTRA, boron-implanted silicon detectors with a 300 mm^2 active surface area and 100 μm depletion depth were used. A nominal FWHM of 16 keV was quoted for each detector.

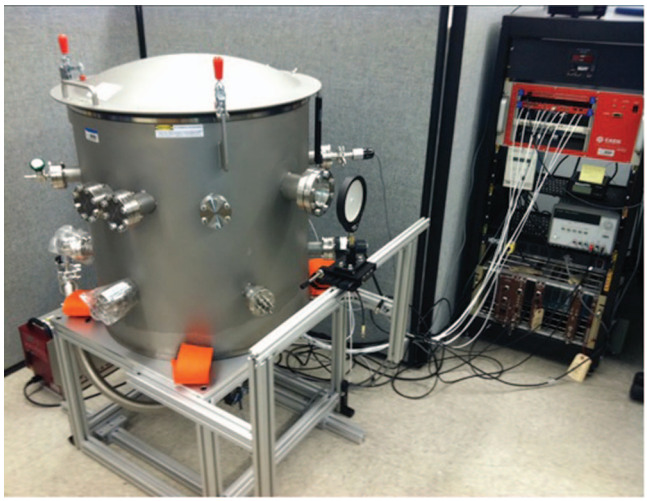

FIG. 3. External view of NDP instrument with digital data acquisition system in testing lab. The turbomolecular pump is located below the chamber with the associated roughing pump. A ^{6}Li neutron aperture sits on an adjustable lens post and linear stage, attached to a rail in front of the chamber. The table supporting the vacuum chamber can be raised or lowered for alignment with the beam, and rest on a set of rails which slide the chamber closer or farther away from the beam shutter. The 14-bit digitizer and associated power supplies can be seen in the electronics rack to the right of the chamber.

Pulses from the detectors are collected on 450 mV/MeV charge sensitive preamplifiers, located in vacuum (Fig. 5). Signals from the preamplifiers are digitized directly after using a 14 bit, 100 MS/s digitizer from CAEN S.p.A. The digitized signal is processed using a trapezoidal filter encoded on a field-programmable gate array (FPGA). The trapezoidal filter for each channel has been optimized to detect the full pulse height, using a 5 μs rise time, 3 μs flattop parameter, and independently determined time constants based on the slightly different decay constant of each channel's preamp. A fiber optic connection relays pulses exceeding a user defined threshold to a PC, where they are stored in list mode. Each filtered pulse is recorded with a timestamp and pulse height in a text file specific to its detector channel. Histogramming and data analysis are performed offline with a user defined histogram bin width. Since data are accumulated in list mode with a timestamp for each event, time resolved histograms can be generated, giving an NDP spectrum for a given time interval during the acquisition.

C. Alignment

Proper alignment of the instrument is vital to ensuring the sample is uniformly irradiated by the most intense portion of the beam, and allowing the beam to pass through the chamber with minimal scattering. Alignment of the instrument was accomplished using an in-house neutron radiography system.[15] Using a ^{6}LiF(ZnS) scintillation screen and aluminized front surface mirror deposited on ^{6}Li-doped glass, a commercial off-the-shelf digital camera was placed perpendicular to the

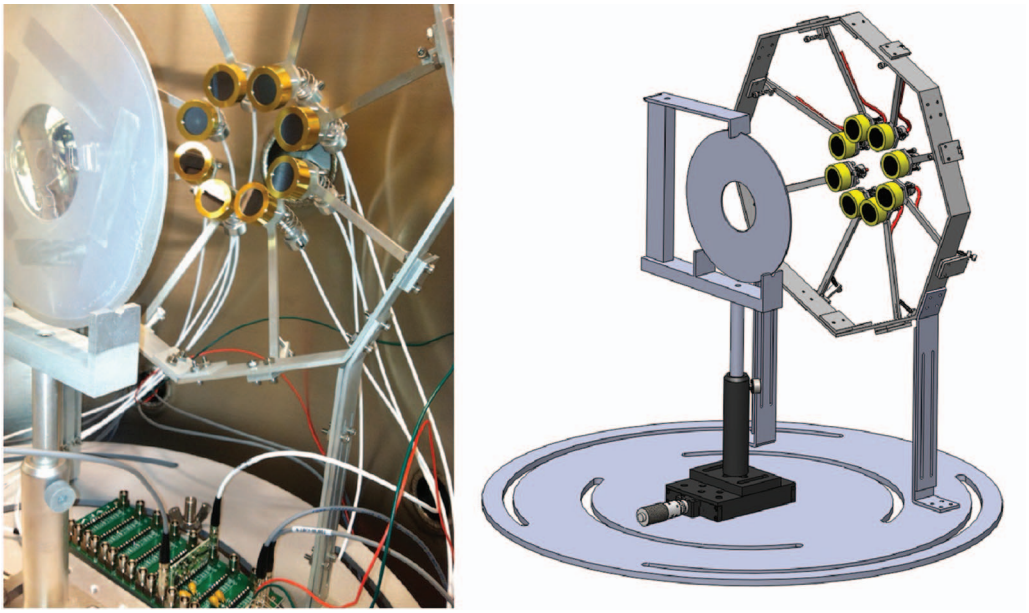

FIG. 4. The 8 detector NDP configuration. Samples are mounted to a teflon sheet in the center of the aluminum disk, and exposed to the neutron beam passing through the center of the detector ring. The distance and angle between detectors and the sample is controlled by adjusting a small screw located on the base of each detector arm.

neutron beam in a light tight box. The exposure time of the camera was adjusted to 64 s using an open-source firmware modification, allowing the camera to capture the mirror reflected image of the screen scintillating.

Positioning of the vacuum chamber was accomplished first. After a rough alignment by sight, the imaging box was placed behind the exit port of the vacuum chamber. A cadmium ruler with 1 cm spaced tick marks was placed on the front of the imaging box for a quantitative measurement of beam location. With the reactor operating at 50 kW thermal power, an image of the entire beam, without the ^{6}Li aperture (see Fig. 2), was taken. The image was processed using a MATLAB script to determine the most intense section of the beam, and the chamber was iteratively repositioned an appropriate distance. Once the entrance and exit ports were positioned concentric to the center of the beam, the vacuum chamber was secured in place.

To align the sample location with the most intense section of the beam, a small Cd cross hair was placed on the center of the sample mount. The imaging device was moved inside of the vacuum chamber, just behind the sample mount. With the reactor running at 50 kW thermal, several images of the beam without the ^{6}Li aperture were taken, allowing the maximum neutron beam footprint to illuminate the sample position. After analyzing the processed images, the height and lateral position of the sample holder were adjusted until the cadmium cross hair was centered in the beam (Fig. 6(a)). Without moving the imaging box or the sample mount, a 10 mm ^{6}Li glass aperture was placed between the vacuum chamber entrance window and beam shutter. The aperture was placed on a linear stage capable of precise movement in the vertical and lateral directions. Several more images were taken with the neutron radiography system, adjusting the location of the aperture after each exposure. After several

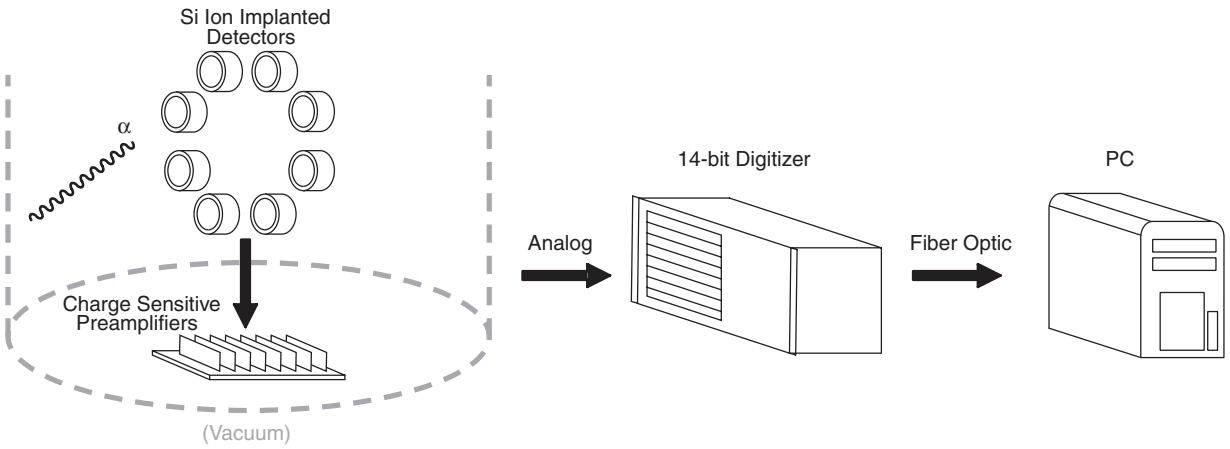

FIG. 5. Signal path of NDP instrument. Analog waveforms are sampled and pass through a programmed FPGA in the digitizer. Pulses above a user defined value are transmitted to a PC via fiber optic connection.

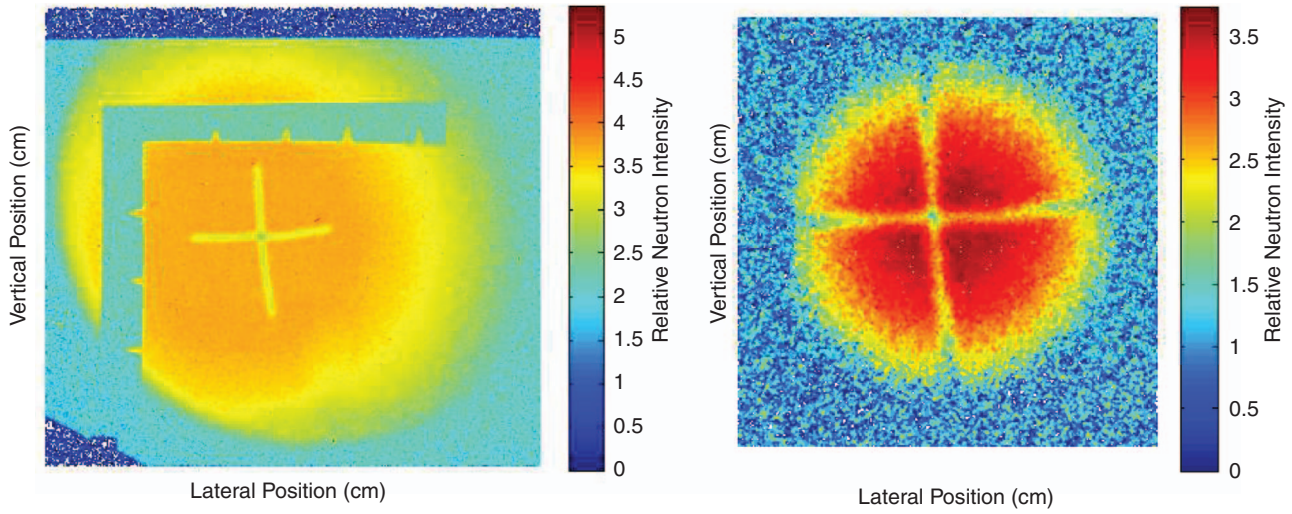

FIG. 6. (a) Processed image of cadmium cross hair sitting at the sample position inside the chamber, aligned with the center of neutron beam. Both images are compared on a logarithmic scale. (b) Processed image of cadmium cross hair centered on sample mount with 10 mm neutron aperture in front of chamber entrance window.

iterations the aperture was properly aligned, circumscribing beam about the center of the Cd cross hair (Fig. 6(b)). Although a 1 cm aperture is placed at the chamber entrance, the beam diverges slightly before reaching the sample location. Preliminary measurements indicate the beam footprint to be 12 mm in diameter at the sample position.

IV. SYSTEM CALIBRATION

Characterizing the gain and solid angle of each detector channel is an important step towards summing the total spectrum. To determine the gain, a spectrum was acquired using an ^{241}Am alpha source. Although a pulser would also be a suitable or perhaps preferable method of determining the system gain, ground loop issues prevented implementation of this technique. Histograms were generated for each detector channel using 4096 bins of varying energy width, depending on the range of data points in the channel. Due to slight differences between preamplifiers, cable lengths, etc., the 5485.6 keV and 5442.8 keV ^{241}Am peaks registered different digital pulse heights in each detector channel. This resulted in significantly different peak widths and locations. To normalize the histogram bin widths between detector channels, such that the energy bin width of one channel matched that of every other channel, a Gaussian distribution was fit to the two peaks in each detector channel using an iterative least squares approximation. This gave a measure of the full width at half max (FWHM), area of each curve, and peak bin number. By determining the analog-to-digital converter (ADC) bin number for each peak, the gain of each detector channel was determined using:

$$\frac{\text{keV}}{ADC\ bin} = \frac{5485.6\ \text{keV} - 5442.8\ \text{keV}}{Peak_1\ Bin - Peak_2\ Bin}. \tag{5}$$

The solid angle of each detector was determined empirically by dividing the area of counts in the 5485.6 keV channel by the product of the activity, branch ratio, and count time of the ^{241}Am source. A summary of the Gaussian fit of each detector channel can be found in Table I.

While the empirically derived solid angles may appear to be significantly smaller for some channels relative to others, it should be noted that the geometry of the source used for this analysis was not ideal. The ^{241}Am was deposited on a thin foil in the bottom of a small well, set back from the surface of a protective plastic disk. This resulted in some shielding for the detectors located on the top of the assembly (channels 1, 2, and 8). A geometrically suitable source with a sufficiently high count rate could not be obtained to verify the solid angles. However, judging by the symmetry of the detector arrangement, the solid angles for channels 1, 2, and 8 should be quite similar to the other five channels.

TABLE I. Characteristics of Gaussian fit for each detector channel.

Channel	keV/ADC bin	FWHM (keV)	5485 keV peak area (counts)	Solid angle
1	0.9853	18.81 ± 0.08	39,862 ± 200	0.011 ± 0.002
2	0.8946	17.84 ± 0.21	42,937 ± 181	0.011 ± 0.002
3	0.9718	19.47 ± 0.45	80,856 ± 284	0.022 ± 0.003
4	0.9398	20.72 ± 0.20	79,235 ± 281	0.021 ± 0.003
5	0.9807	20.41 ± 0.74	82,820 ± 288	0.022 ± 0.003
6	0.9830	19.65 ± 0.84	81,488 ± 285	0.022 ± 0.003
7	1.030	22.12 ± 1.33	73,773 ± 272	0.020 ± 0.003
8	0.9875	26.35 ± 1.02	56,725 ± 238	0.015 ± 0.002

V. CHANNEL SUMMING

A. ^{241}Am spectrum

As most NDP instruments analyze the spectrum obtained from a single detector, one must look to other areas for precedence in summing multiple spectra. In gamma-ray spectroscopy, two methods have been developed to add spectra obtained from different systems with gain variations. The goal of each method is to reconstruct the distribution of data points within a histogram bin, usually by fitting a polynomial

function across adjacent bins, such that the counts in one bin can be redistributed, deterministically[16] or stochastically,[17] across a new bin of arbitrary width. Once two or more histograms have been redistributed to a common scale, they can be summed quite easily. One of the advantages of acquiring data in list mode is that events are recorded individually. In this sense, the position of a count within an energy bin is retrievable, while it is not with the traditional analog MCA. This allows the user to generate a histogram of arbitrary bin width without degrading the statistical significance of the spectrum. This is the principle behind the spectrum summing technique employed in our instrument.

While it may seem that an infinitely narrow bin width may be used to generate a histogram from the listed data, this is not the case. Using an increasingly fine histogram could result in more background counts accumulating in a single historgram bin than counts due to the signal, degrading the resolution of the spectrum. However, in the case of this instrument, the minimum histogram bin width is bounded by the inherent limitations of the digitizer. Due to floating point round-off in the digitizer, pulse heights do not occupy a continuous range of values. When a histogram was generated using bin widths less than approximately 0.7 keV, empty bins appeared periodically throughout the spectrum. Thus, 0.7 keV has been determined to be the lower limit of the user defined histogram bin width for this instrument.

After determining the gain of each detector channel, the list data were distributed in a histogram, with each bin having equal energy width. This placed an equal number of bins between the two ^{241}Am peaks for each detector channel. The histograms were then aligned to the 5485.6 keV peak of each channel and summed. Results of the alignment of two peaks from ^{241}Am between detector channels can be seen in Fig. 7, along with the spectrum obtained from summing all 8 channels. As the figure indicates, the detector channels aligned quite close to one another with minimal broadening. This resulted in a summed spectrum having the two Am peaks clearly discernible. A Gaussian distribution fit to the summed spectrum indicated a FWHM of 21.30 ± 0.30 keV.

B. Lithium scintillator sample

As a preliminary test, a section of lithium scintillation screen was placed in the instrument and analyzed. The scintillation screen (i.e., a neutron imager) was a mixture of ^{6}LiF and phosphor manufactured by Applied Scintillation Technologies, with a thickness of approximately 0.3 mm, infinitely thick with respect to the range of the most energetic charged particle (2727 keV triton). The sample was analyzed at the OSURR operating at 450 kW thermal power, using a 30 mm beam aperture. A spectrum was acquired for approximately 61 min in list mode using all 8 detectors. The data for each detector channel were then distributed in separate histograms using a multiple of the previously determined channel gain as bin widths. Significant low energy noise was present in the signal and warranted a background subtraction before summing the spectra. A background count was obtained with the reactor operating at 450 kW and an empty sample mount. The scintillator and background spectra for each detector channel were then normalized to their respective count times and subtracted. Each detector channel was then aligned by first applying a Savitzky-Golay smoothing filter to each histogram. A differential filter was applied to the smoothed histogram, and the zero crossing of the leading edge of each spectrum was used as a reference to align each channel. All detector channels were then aligned to the channel with the leading edge nearest zero. After shifting each histogram, the spectra were summed. As Fig. 8 indicates, the 2727 keV triton peak and 2055 keV alpha peak were visible above the low energy noise, making ^{6}Li a suitable candidate for further NDP studies of Li-containing thin-film materials at the OSURR. The spectrum also indicates that the majority of the Li in the scintillator material is located on the surface, with a smaller but constant distribution throughout. This is evidenced by the sharp triton peak at 2727 keV and relatively flat spectrum at lower energies (i.e., where neutron absorption took place deeper below the surface).

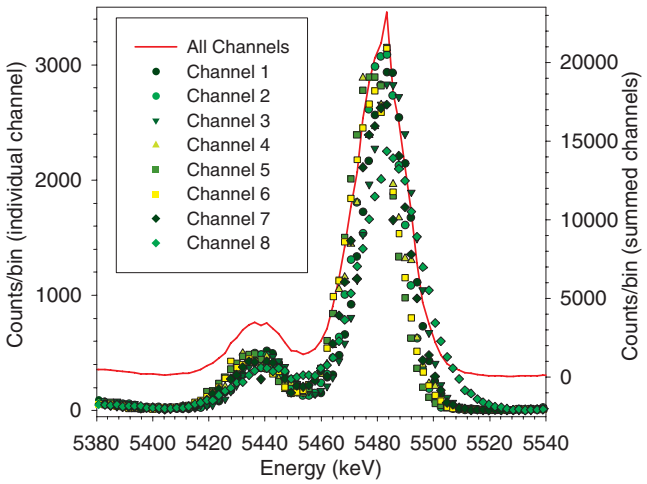

FIG. 7. ^{241}Am spectrum acquired from each independent channel, showing 5485.6 keV and 5442.8 keV peaks. The summed spectrum is also shown in red.

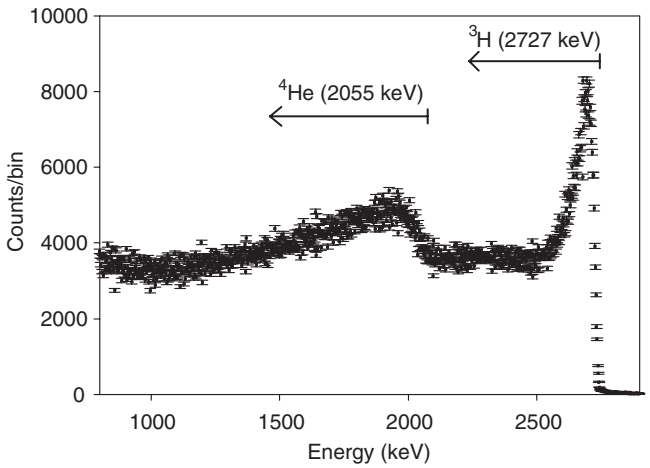

FIG. 8. Peaks of interest obtained from the ^{6}Li(n,^{3}H)^{4}He reaction in scintillation screen with background subtracted.

C. Calibration standard

To benchmark the multi-detector design, a borophosphosilicate glass (BPSG) standard analyzed at the NDP facility at the National Institute of Standards and Technology (NIST) Center for Neutron Research (CNR) was used. The NIST NDP facility shares a cold neutron beam cooled by a liquid hydrogen neutron source in a 20 MW research reactor, with a thermal equivalent flux of 7.6×10^8 n/cm^{-2} s^{-1} at the target location.[18] This high neutron flux, combined with low gamma contamination in the neutron beam, results in higher counting rates and reduced low energy noise when performing NDP.

After analyzing the BPSG standard at NIST, the standard was analyzed at the OSURR, operating at 450 kW thermal power. A 30 mm neutron aperture was used, and the sample was counted for 54 min. A background spectrum was obtained by opening the beam shutter with nothing in the sample mount. After normalizing the BPSG and background spectra to their respective count times, the background was subtracted (Fig. 9). Each detector channel was aligned in a manner similar to the method used for the scintillation screen. After relocating each detector spectra, the channels were summed.

As previously mentioned, the NDP spectrum acquired in list mode is distributed in a histogram according to a user defined bin width. By choosing a broader bin width, more counts fall between the bounds of each histogram bin. With more counts in each bin, the relative uncertainty of a measurement is decreased, and fluctuations in the spectrum tend to converge. To demonstrate this principle, the BPSG spectrum obtained at the OSURR was analyzed using a 1 keV and 2.1 keV bin width. While a user could generate a histogram using increasingly smaller energy bins, widths below 0.7 keV result in spectrum gaps, due to floating point round off in the digitizer.

To assess the quality of the 8 summed spectra, a plot of the NDP spectrum obtained at NIST with the same BPSG is featured in Fig. 10. As the figure indicates, the 1472 keV alpha peak of the multi-detector device and the NIST device align quite closely and are very distinct from any noise. The 840 keV ^{7}Li peak is less defined and encounters low energy noise much sooner than the NIST spectrum. However, since only one of the products of the neutron induced reactions are necessary to determine a depth profile, the alpha peak can be unfolded by itself. Figure 11 depicts the depth profile determined from the NIST and OSURR spectrum. As the figure shows, the multi-detector instrument is capable of achieving a count rate nearly half that of NIST's instrument, in spite of a significantly lower neutron flux.

While a higher count rate is obtained by using more detectors, fluctuations in the spectrum are more pronounced in this setup. This could be due to the limited count time available for data acquisition. Collecting data over longer periods of time could help to smooth these fluctuations, and will be attempted in future work.

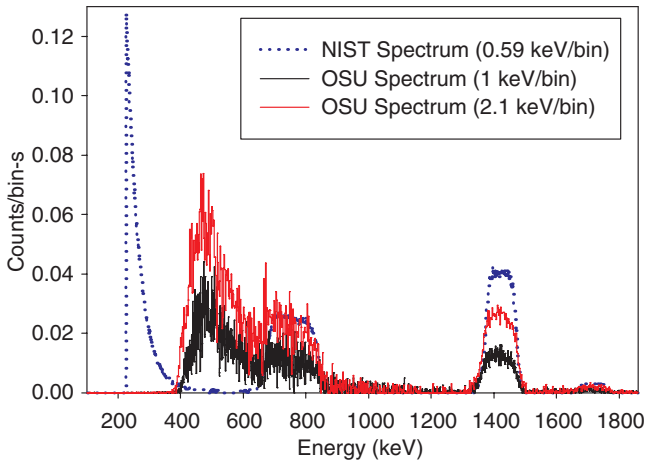

FIG. 10. BPSG spectrum obtained from NIST analysis, compared with the spectrum obtained at the OSURR using multiple detectors. By altering the histogram bin width to 2.1 keV/bin, nearly half the count rate of NIST is achievable.

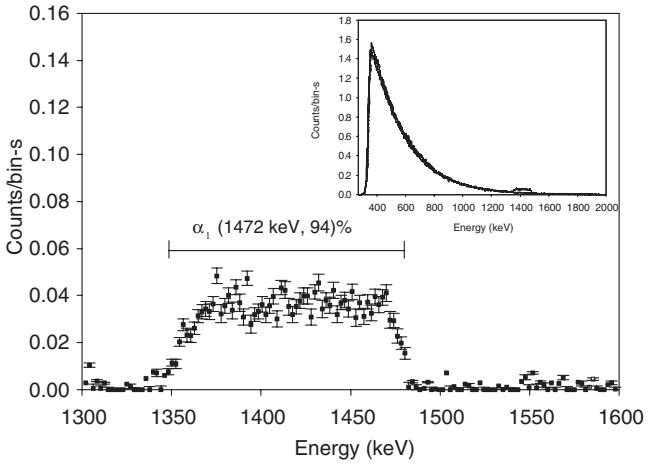

FIG. 9. A singe detector channel analyzing the ^{10}B(n,^{4}He)^{7}Li reaction in BPSG. The broadened 1472 keV α_1 peak is distinct above background, and can be used to determine the ^{10}B concentration as a function of depth. The inset figure shows the background (thin line) and BPSG spectrum (thick line) plotted together. The substantial low energy noise prevents the 840 keV ^{7}Li nucleus from being used in NDP analysis.

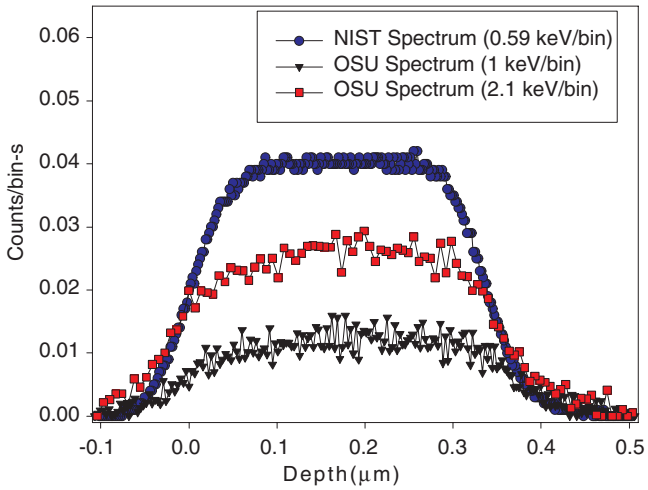

FIG. 11. BPSG count rate as a function of depth obtained at NIST and OSURR. While there are more fluctuations in the OSURR data, longer counting times could smooth the variations between these points.

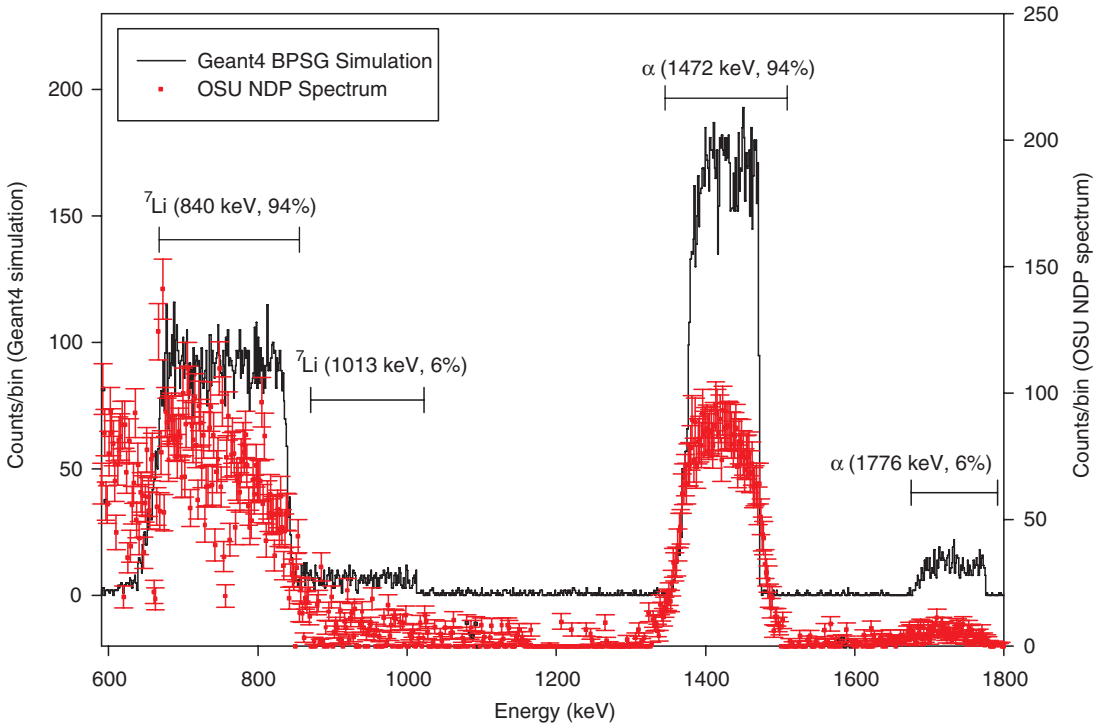

FIG. 12. Geant4 simulation of BPSG spectrum against OSU experimental BPSG spectrum. While the 94% branch ratio α particle is distinguishable in the experimental spectrum, the lower branch ratio ^{7}Li and α particles are masked by the background. Similarly, the 94% ^{7}Li recoil nucleus is obstructed by low energy noise.

As a second means of validating our instrument, a model using the Geant4 toolkit[19] was created to simulate a BPSG spectrum. A 330 nm thick section of BPSG with a uniform boron distribution was bombarded with neutrons following a Maxwell-Boltzmann energy distribution. Charged particles were detected using a 300 mm^2 disk of Si in a vacuum environment. When comparing the noisy spectrum obtained from the OSURR to the Geant4 simulation, it is evident that the lower branch ratio peaks are lost in the system noise (Fig. 12). However, examination of the ^{4}He peak shows good agreement between the experimental and theoretical spectra.

VI. CONCLUSIONS

A multi-detector NDP instrument has been constructed and has obtained a depth profile spectrum from several samples using digital instrumentation. By way of the multiple detectors, this instrument is capable of achieving a relatively high count rate for a low power research reactor. However, this higher count rate comes at the expense of energy resolution. While the relationship between a higher count rate and energy resolution is not directly causal, there is some loss of resolution when all 8 channels are summed together, due to the inclusion of less resolved channels. Low energy noise presents a problem with this instrument, which is most likely due to gamma contamination in the neutron beam.

ACKNOWLEDGMENTS

The authors would like to acknowledge the assistance of Greg Downing at NIST, Marco Locatelli at CAEN S.p.A, and Joseph Talnagi, Andrew Kauffman, and Kevin Herminghuysen at the OSU Research Reactor in the completion of this work. This work is partially supported by the U.S. Nuclear Regulatory Commission award for The Ohio State University Nuclear Engineering Faculty Development Program.

[1] J. F. Ziegler, G. W. Cole, and J. E. E. Baglin, J. Appl. Phys. **43**(9), 3809 (1972).
[2] J. P. Biersack, D. Fink, R. Henklemann, and K. Muller, Nucl. Instrum. Methods. Phys. Res. **149**, 93 (1978).
[3] R. G. Downing, G. P. Lamaze, J. K. Langland, and S. T. Hwang, J. Res. Natl. Inst. Stand. Technol. **98**, 109 (1993).
[4] H. H. Chen-Mayer, D. F. R. Mildner, G. P. Lamaze, R. L. Paul, and R. M. Lindstrom, AIP Conf. Proc. **475**, 718 (1999).
[5] V. Havránek, V. Hnatowicz, J. Kvítek, J. Vacík, and J. Hoffmann, Nucl. Instrum. Methods Phys. Res. B **73**, 523 (1993).
[6] J. Vacík, J. Červená, V. Hnatowicz, V. Havránek, J. Hoffmann, S. Pošta, D. Fink, and R. Klett, Nucl. Instrum. Methods Phys. Res. B **142**, 397 (1998).
[7] S. M. Çetiner and K. Ünlü, Nucl. Instrum. Methods Phys. Res. **579**(1), 148 (2007).
[8] V. T. Jordanov and G. F. Knoll, Nucl. Instrum. Methods Phys. Res. A **345**, 337 (1994).
[9] J. F. Ziegler, M. D. Ziegler, and J. P. Biersack, Nucl. Instrum. Methods Phys. Res. **268**(11–12), 1818 (2010).
[10] J. K. Shultis, Nucl. Instrum. Methods Phys. Res. **526**(3), 359 (2004).
[11] J. T. Maki, R. F. Fleming, and D. H. Vincent, Nucl. Instrum. Methods Phys. Res. B **17**, 9 (1986).
[12] K. J. Coakley, IEEE Trans. Nucl. Sci. **38**(1), 7 (1991).
[13] V. Hnatowicz, J. Vacik, and D. Fink, Rev. Sci. Instrum. **81**(7), 8 (2010).
[14] D. Turkoglu, J. Burke, R. Lewandowski, and L. R. Cao, J. Radioanal. Nucl. Chem. **291**, 321 (2012).
[15] R. Lewandowski, L. R. Cao, and D. Turkoglu, Nucl. Instrum. Methods Phys. Res. **674**, 46 (2012).
[16] L. Loska, Appl. Radiat. Isot. **46**, 949 (1995).
[17] S. P. Tsai, E. R. Mucciolo, and O. Helene, Nucl. Instrum. Methods Phys. Res. A **345**, 538 (1994).
[18] R. G. Downing, personal communication (2012).
[19] S. Agostinelli *et al.* Nucl. Instrum. Methods Phys. Res. **506**(3), 250 (2003).